This article has been accepted for publication in a future issue of this journal, but has not been fully edited. Content may change prior to final publication. Citation information: DOI 10.1109/TPWRD.2016.2536704, IEEE Transactions on Power Delivery

Eliminating Measurement Cable Effects From Transformer Admittance Measurements

Bjørn Gustavsen, *Fellow, IEEE*

***Abstract*—Admittance frequency sweep measurements is an accepted procedure for characterizing transformer terminal behavior for the purpose of frequency-dependent black-box modeling. The errors introduced by the measurement cables is with one existing practice mitigated by removal of the associated shunt capacitance effect. In this work it is shown that the accuracy can be greatly improved by usage of a transmission line representation of the measurement cables with parameters obtained from standard cable data or from S-parameter measurements. The procedure is demonstrated for the modeling a 45 MVA generator step-up transformer requiring cable lengths of six meters and an upper frequency limit of 10 MHz.**

***Index Terms*—Transformer, model, wide-band, black box, measurement, cable compensation.**

I. Introduction

FREQUENCY sweep measurements is a convenient way of characterizing the behavior of complex network components like transformers over a wide frequency band. Such measurements aim at describing the component's terminal behavior in terms of scattering [1] or admittance parameters [2-5], or voltage transfer functions [6]. By subjecting the obtained frequency domain description to fitting with rational functions, a black-box model of the component is obtained which can be interfaced [7] with electromagnetic transient programs [8] for simulation of general network interaction, including resonances and voltage transfer between windings [9-12].

Some transformer measurement setups are based on direct measurement of the transformer's admittance matrix with the required short-circuits realized on a connection box that is attached to the transformer terminals through (shielded) measurement cables. The cables influence the measured result, in particular at high frequencies. In [3], it was proposed to remove the cable effects by subtracting the cable shunt admittances from the associated diagonal elements of the measured admittance matrix. This procedure was demonstrated to give good results for cables up to 5-m length, for frequencies up to 1 MHz. For simulation of very fast transients, however, it may be necessary to extend the modeling beyond the 1 MHz range, and it may also be necessary to use longer cables.

This work demonstrates that removal of capacitance effects alone is insufficient if the goal is to consider frequencies up to 10 MHz and cables in excess of 5 m length. A new cable compensation method is introduced which is based on a transmission line representation of the measurement cables. It is shown how to obtain the line representation using either cable standard parameters or *S*-parameter measurements. The new compensation method is applied to an actual case where 45 MVA generator step-up transformer is to be modeled in the range 5 Hz-10 MHz using cables of 5 m and 6 m length. The obtained result is compared to that obtained with direct measurements using very short measurement cables, both in the frequency domain and in the time domain. The improvements over capacitive compensation are highlighted. The new compensation method was already used by this author in [11] and later works, but it was never documented.

II. Admittance Modeling and Measurements Cables

The transformer is to be represented by its admittance matrix $\mathbf{Y}_T$ which relates terminal voltages $\mathbf{v}_T$ and terminal currents $\mathbf{i}_T$,

$$\mathbf{i}_T(\omega) = \mathbf{Y}_T(\omega)\mathbf{v}_T(\omega) \tag{1}$$

$\mathbf{Y}_T$ is measured using a suitable setup, e.g. as described in [3], and finally subjected to modeling by a stable and passive rational model,

$$\mathbf{Y}_T(\omega) \cong \tilde{\mathbf{Y}}_T(\omega) = \mathbf{R}_0 + j\omega\mathbf{R}_{-1} + \sum_{j=1}^{N} \frac{\mathbf{R}_j}{j\omega - a_j} \tag{2}$$

The transformer is connected to the measurement box using shielded cables. The cable shields are grounded at both ends, on the connection box and on the transformer. At high frequencies, the current in each cable conductor returns in the metallic shield, eliminating any mutual coupling between the cables. Accordingly, each cable can be modeled separately as a single-conductor two-terminal transmission line. The cable behavior is governed by its length *l*, and its per-unit-length (p.u.l.) series impedance *Z* and shunt admittance *Y*,

$$Z(\omega) = R(\omega) + j\omega L(\omega) \tag{3a}$$

$$Y(\omega) = G(\omega) + j\omega C(\omega) \tag{3b}$$

Manuscript received April 29, 2015.

B. Gustavsen is with SINTEF Energy Research, N-7465 Trondheim, Norway (e-mail: bjorn.gustavsen@sintef.no).

This work was supported by the Norwegian Research Council (RENERGI Programme) with additional support from DONG Energy, EirGrid, Hafslund Nett, National Grid, Nexans Norway, RTE, Siemens Wind Power, Statnett, and Statkraft.

This article has been accepted for publication in a future issue of this journal, but has not been fully edited. Content may change prior to final publication. Citation information: DOI 10.1109/TPWRD.2016.2536704, IEEE Transactions on Power Delivery

One normally assumes *G* to be zero and *C* independent of frequency.

III. Cable Elimination Considering Shunt Capacitance Effect

In the approach proposed in [3], *Z* is ignored. As a result, the shunt admittance (3b) adds directly to the diagonal elements of $\mathbf{Y}_{\mathrm{T}}$ in (1) and the admittance of the transformer alone is recovered by subtracting from the diagonal elements of the measured admittance matrix $\mathbf{Y}_{\mathrm{meas}}$ the cable shunt admittance,

$$\mathbf{Y}_{\mathrm{T}}^{(i,i)}(\omega) = \mathbf{Y}_{\mathrm{meas}}^{(i,i)}(\omega) - j\omega(C^i \cdot l^i) \tag{4}$$

with *i* indicating the cable connected to the *i*th terminal.

This approximation is expected to be sufficiently accurate as long as the voltage does not vary substantially along the cable and the cable series impedance is small compared to the transformer input impedance. This cable elimination method will in the following be referred to as the *Cap-method*.

IV. Cable Elimination Considering Transmission Line Effect

A. Approach

For each cable the familiar two-terminal admittance matrix applies,

$$\mathbf{Y}_{\mathrm{cable}}(\omega) = \begin{bmatrix} a(\omega) & b(\omega) \\ b(\omega) & a(\omega) \end{bmatrix} \tag{5}$$

where

$$a(\omega) = \frac{\coth(\gamma(\omega)l)}{Z_C(\omega)} \tag{6a}$$

$$b(\omega) = \frac{-1}{Z_C(\omega)\sinh(\gamma(\omega)l)} \tag{6b}$$

and

$$Z_C(\omega) = \sqrt{\frac{Z(\omega)}{Y(\omega)}} \tag{7}$$

$$\gamma(\omega) = \sqrt{Z(\omega)Y(\omega)} \tag{8}$$

The relation between the measured admittance, $\mathbf{Y}_{\mathrm{meas}}$, and the transformer admittance $\mathbf{Y}_{\mathrm{T}}$ can be analyzed using the circuit topology in Fig. 1,

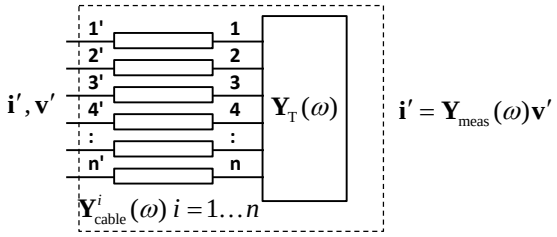

Fig. 1. Circuit topology relating transformer admittance matrix $\mathbf{Y}_{\mathrm{T}}$ with measured admittance matrix $\mathbf{Y}_{\mathrm{meas}}$.

To see how the measurement cables can be eliminated, each cable is represented by its exact PI-equivalent as shown in in Fig. 2,

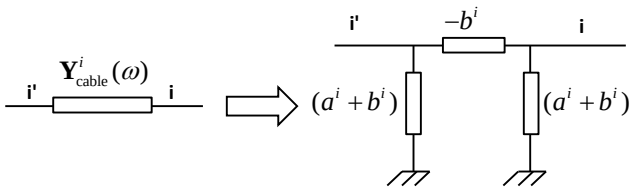

Fig. 2. PI-model of *i*th cable.

and it is observed that the cable effect becomes eliminated when connecting in series a PI-section with *negated* elements as shown in Fig. 3. This cable elimination method will in the following be referred to as the *T-line method*.

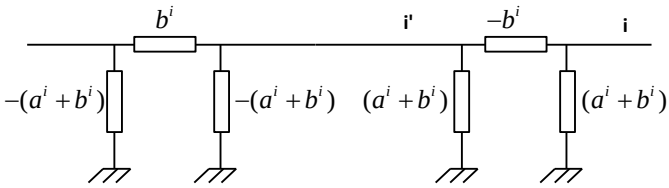

Fig. 3. Elimination of *i*th cable.

B. Elimination of Internal Nodes

The internal nodes in Fig. 3 are finally eliminated using standard Kron reduction [13] as follows.

The $2n \times 2n$ admittance matrix $\mathbf{Y}_{\mathrm{aug}}$ of the circuit in Fig. 4 is established using standard nodal analysis whereby the admittance stamp of each component (transformer, measurement cables) are added into $\mathbf{Y}_{\mathrm{aug}}$. With the *n* external nodes numbered first, the following partitioning of $\mathbf{Y}_{\mathrm{aug}}$ results,

$$\mathbf{Y}_{\mathrm{aug}}(\omega) = \begin{bmatrix} \mathbf{Y}_A & \mathbf{Y}_B \\ \mathbf{Y}_C & \mathbf{Y}_D \end{bmatrix} \tag{9}$$

Since the current injection from ground to the *n* internal nodes is zero, the lower matrix equation in (9) is zero. From this condition one obtains from (9) the $n \times n$ admittance with respect to the *n* external nodes as

$$\mathbf{Y}_{\mathrm{ext}}(\omega) = \mathbf{Y}_A - \mathbf{Y}_B\mathbf{Y}_D^{-1}\mathbf{Y}_C \tag{10}$$

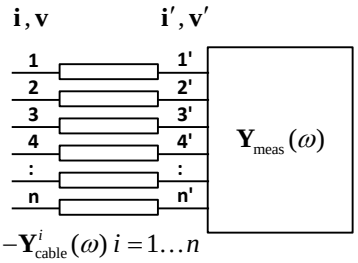

Fig. 4. Circuit used for recovering $\mathbf{Y}_{\mathrm{T}}$ from $\mathbf{Y}_{\mathrm{meas}}$.

V. Cable Parameter Determination

A. Standard Cable Data

Measurement cables are typically specified by their characteristic impedance Z_{C} and capacitance per unit length, *C*. The cable inductance per unit length can now be obtained

This article has been accepted for publication in a future issue of this journal, but has not been fully edited. Content may change prior to final publication. Citation information: DOI 10.1109/TPWRD.2016.2536704, IEEE Transactions on Power Delivery

as

$$L = C \cdot Z_C^2 \tag{11}$$

The resistance can be measured, e.g. using an impedance analyzer, or be set to an assumed value, e.g. zero. Also, G can be assumed zero. With this information, $\mathbf{Y}_{\text{cable}}(\omega)$ in (5) can be calculated for each measurement cable.

B. S-parameter Measurements

It is also possible to determine $\mathbf{Y}_{\text{cable}}(\omega)$ in (5) using two-port S-parameter measurements. Here, one measures the matrix

$$\mathbf{S}(\omega) = \begin{bmatrix} S_{11} & S_{12} \\ S_{21} & S_{22} \end{bmatrix} \tag{12}$$

which relates incident (**a**) and reflected (**b**) power waves,

$$\mathbf{b} = \mathbf{S}\,\mathbf{a} \tag{13}$$

S is a symmetrical matrix (S_{21}=S_{12}) and one also has S_{11}=S_{22} due to the symmetry with respect to the two cable ends.

The scattering matrix is finally converted into admittance parameters through the transformation [14],

$$\mathbf{Y}(\omega) = \mathbf{R}_0^{-1/2}(\mathbf{I} - \mathbf{S}(\omega))(\mathbf{I} + \mathbf{S}(\omega))^{-1}\mathbf{R}_0^{-1/2} \tag{14}$$

where **I** is the 2×2 identity matrix and $\mathbf{R}_0$ is a diagonal matrix holding the two reference resistances; in this work 50 Ω.

VI. Considerations to Accuracy and Passivity

A. Accuracy

A theoretical comparison of the two cable compensation schemes is performed for measurement cables of 6-m length using the cable admittance matrix defined by (5), assuming frequency-independent p.u.l. parameters. The cable characteristic impedance and capacitance are assumed to be Z_C=50 Ω and C=105 pF/m which by (11) gives a series inductance L=0.263 μH/m. The cable resistance (conductor plus screen return) is assumed to be 0.001 Ω/m.

At high frequencies, the transformer input impedance is much higher than the cable characteristic impedance. The two cable compensation schemes are therefore applied to the measurement cable when terminated by an infinite impedance at the far end. The admittance seen into the sending end is obtained from (5) by elimination of the far end node,

$$Y_{\text{send}}(\omega) = a(\omega) - \frac{b^2(\omega)}{a(\omega)} \tag{15}$$

An ideal cable compensation method should now give zero admittance seen into the sending end. The lowest resonance frequency associated with the sending end admittance is that of the cable quarter-wave resonance (16), which is a series resonance. A cable length l=6 m gives a resonance frequency $f_{\lambda/4}$=7.9 MHz. At twice this frequency (15.8 MHz), a parallel resonance occurs which appears as an anti-resonance in an admittance plot.

$$f_{\lambda/4} = \frac{1}{4\tau} = \frac{v}{4l} = \frac{1}{4l\sqrt{LC}} \tag{16}$$

Fig. 5 shows the admittance seen into the cable end when attempting to eliminate the cable using the *Cap-method*. At low frequencies (below 1 MHz) the method gives the desired result of a near zero admittance (infinite impedance). However, with increasing frequency the method fails completely in eliminating the cable effects.

Fig. 6 shows the corresponding result when using the *T-line method*. This approach gives as expected a perfect compensation of the cable provided that the cable parameters are accurately known. The figure shows the result for alternative estimates R_{est} of the p.u.l. series resistance used in the compensation scheme. It is observed that even when using a resistance which is ten times too small, the error remains quite moderate.

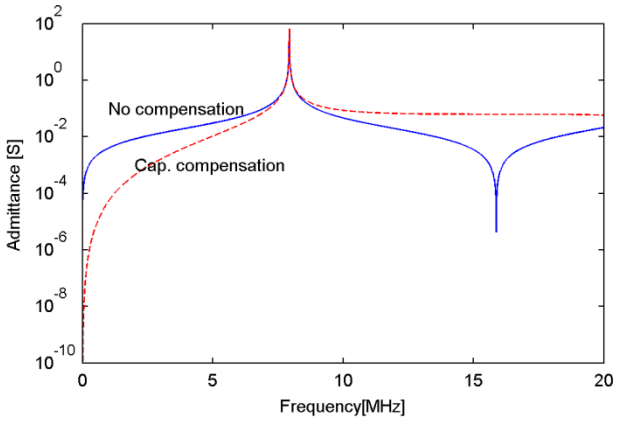

Fig. 5. Cable elimination using *Cap method*. Admittance seen into sending end of a 6-m open-ended cable.

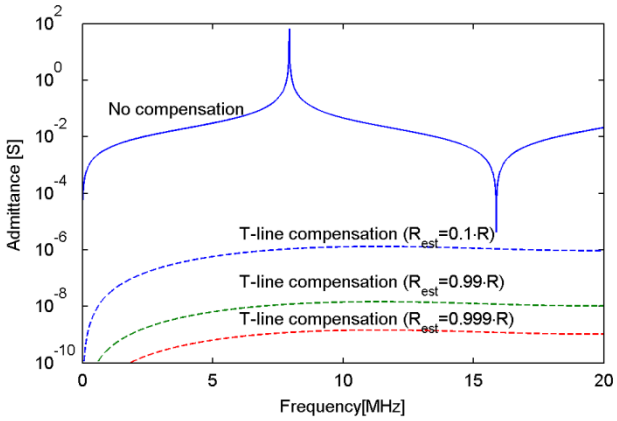

Fig. 6. Cable elimination using *T-line method*. Admittance seen into sending end of a 6-m open-ended cable having resistance R=0.001 Ω/m. Alternative values (R_{est}) for assumed cable resistance.

B. Passivity

The final model of the transformer is required to be passive in order to guarantee a stable time domain simulation. Passivity entails that the Hermitian part of the model's admittance matrix $\tilde{\mathbf{Y}}_T$ in (2) has positive eigenvalues (17). In addition, $\mathbf{R}_{-1}$ is required to have positive eigenvalues. It is essential that the cable compensation does not lead to passivity violation in the data and thus the model that is to be extracted.

This article has been accepted for publication in a future issue of this journal, but has not been fully edited. Content may change prior to final publication. Citation information: DOI 10.1109/TPWRD.2016.2536704, IEEE Transactions on Power Delivery

$$\lambda_k\{(\tilde{\mathbf{Y}}_T(\omega)+\tilde{\mathbf{Y}}_T^H(\omega))\}>0\ \forall\ \omega, k=1\ldots n \qquad (17)$$

With the *Cap method*, one subtracts a fixed capacitance $j\omega\mathbf{C}$ from the terminal admittance. It may easily happen that an extracted model will get a capacitance matrix ($\mathbf{R}_1$ in (2)) with one or more negative eigenvalues, thereby violating the passivity condition. The subsequent passivity enforcement by perturbation may then lead to non-negligible errors in the final model. This problem is in particular relevant for the combination of long measurement cables and a high upper frequency limit.

With the *T-line method*, passivity violations may also result if the cable parameters are not accurately known. Fortunately, the cable capacitance is normally specified by the manufacturer and the inductance can be calculated by (11) using the cable characteristic impedance specified by the manufacturer. In this situation, the cable resistance is not likely to give passivity violations as long as it is specified as smaller than (or equal to) the true resistance. A safe choice is therefore the cable DC resistance. Alternatively, one may use a frequency-dependent resistance (and inductance) for the cable, calculated directly from the cable geometry [15].

VII. Application to Transformer Modeling

The two procedures (*Cap-method*, *T-line method*) are in the following demonstrated for the modeling of a transformer from frequency sweep measurements. With the *T-line method*, the cable admittance representation is determined via standard cable data. In Section VIII, some results are shown when determining the cable model via *S*-parameter measurements.

A. Transformer Measurements

The unit is a 45 MVA YNd11 three-phase two-winding generator transformer which steps the voltage up from 8.5 kV to 137 kV. A pole-residue model (2) is to be extracted based on frequency sweep measurements by a setup similar to the one in [3].

The terminal admittance matrix was measured from 5 Hz to 10 MHz using long cables, giving a 6×6 matrix $\mathbf{Y}_{\text{meas}}^{(\text{long})}$. The measurements used RG214 cables with Z_C=50 Ω. The cable lengths are given in Table I along with measured capacitances.

Table I.
Cable Lengths in First Measurement. (Long Cables)

Winding	HV			LV		
Phase #	A	B	C	a	b	c
Cable #	1	2	3	4	5	6
C [pF/m]	104	105	105	102	102	102
l [m]	6.2	6.0	6.2	4.8	5.1	4.9

From Z_C and and the p.u.l. capacitances in Table I, the inductance is calculated for each cable using (11). With cable lengths l=6.0 m and l=5.0 m one obtains from (16) a quarter-wave resonance frequency $f_{\lambda/4}$=8 MHz and 10 MHz, respectively. These resonance frequencies fall within the 10 MHz upper frequency limit of the measurement. A cable resistance of R=0.001 Ω/m is assumed in lack of other data.

In order to validate the two cable compensation approaches, new measurements were performed on the transformer with reduced cable lengths as shown in Table II. The new matrix associated with the six terminals is denoted $\mathbf{Y}_{\text{meas}}^{(\text{short})}$. Terminals 1, 2, 4, 5 were directly grounded on the transformer while terminals 3 and 6 had short cables (1.0 m) used for measuring a 2×2 subset of $\mathbf{Y}_{\text{meas}}^{(\text{short})}$ associated with those two terminals. The objective is now to recover the elements of $\mathbf{Y}_{\text{meas}}^{(\text{short})}$ by applying the cable elimination methods to $\mathbf{Y}_{\text{meas}}^{(\text{long})}$.

Table II.
Cable Lengths in Second Measurement. (Short Cables)

Winding	HV			LV		
Phase #	A	B	C	a	b	c
Cable #	1	2	3	4	5	6
C [pF/m]	–	–	105	–	–	105
l [m]	0	0	1.0	0	0	1.0

Figs. 7-9 show the four elements of $\mathbf{Y}_{\text{meas}}^{(\text{long})}$ and of $\mathbf{Y}_{\text{meas}}^{(\text{short})}$ associated with terminals 3 and 6, in the range 100 kHz-10 MHz. It is observed that the length of the measurement cables has a significant impact on the measured admittance elements. Element (3,3) is in particular affected since the high-voltage winding has a smaller shunt capacitance to ground than the low-voltage winding. Also, there is with the long cable a strong resonance peak in element (3,3) at around 8 MHz which can be attributed to quarter-wave resonance in the connected cable.

Figs. 7-9 further show the recovering of the four elements of $\mathbf{Y}_{\text{meas}}^{(\text{short})}$ from $\mathbf{Y}_{\text{meas}}^{(\text{long})}$ by the two alternative cable compensation methods, considering the reduction in cable lengths defined by Tables I and II. It is observed that the T-line method gives a much better overall agreement with the directly measured $\mathbf{Y}_{\text{meas}}^{(\text{short})}$ (reference) than the Cap-method. With the Cap-method, only the diagonal elements of $\mathbf{Y}_{\text{meas}}^{(\text{long})}$ are modified and there is accordingly no change in the off-diagonal elements in Fig. 9. It is further observed that the CAP-method is not capable of removing the false peak in element (3,3) at 8 MHz in Fig. 7, consistently with the result in Fig. 5.

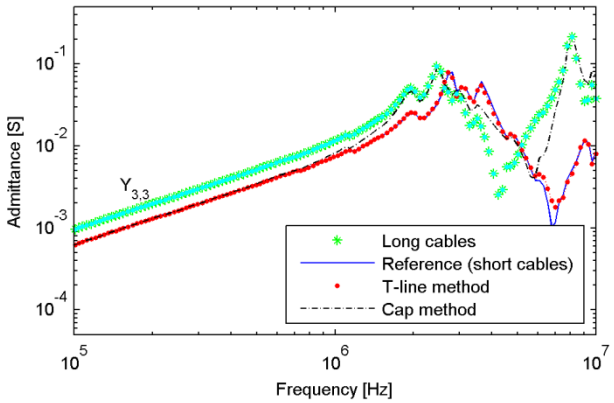

Fig. 7. Recovering element (3,3) of $\mathbf{Y}_{\text{meas}}^{(\text{short})}$ from $\mathbf{Y}_{\text{meas}}^{(\text{long})}$.

This article has been accepted for publication in a future issue of this journal, but has not been fully edited. Content may change prior to final publication. Citation information: DOI 10.1109/TPWRD.2016.2536704, IEEE Transactions on Power Delivery

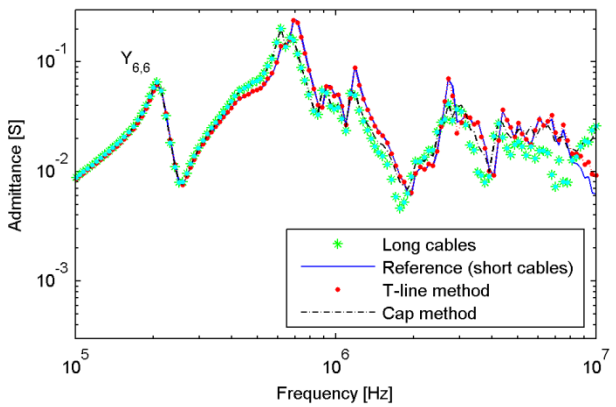

Fig. 8. Recovering element (6,6) of $\mathbf{Y}_{\text{meas}}^{(\text{short})}$ from $\mathbf{Y}_{\text{meas}}^{(\text{long})}$.

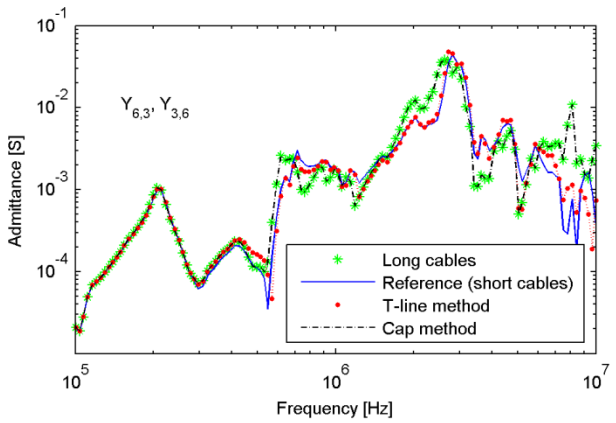

Fig. 9. Recovering elements (6,3) and (3,6) of $\mathbf{Y}_{\text{meas}}^{(\text{short})}$ from $\mathbf{Y}_{\text{meas}}^{(\text{long})}$.

B. Voltage Transfer Functions

The significance of accurately recovering the transformer admittance matrix is demonstrated for a calculation of voltage transfer functions between terminals. Fig. 11 shows a direct measurement of the voltage transfer function $h_{6,3}(\omega)$ from terminal 3 to terminal 6 using the cable lengths in Table II with the remaining terminals grounded. The voltage transfer function is defined as

$$h_{6,3}(\omega) = \frac{V_6(\omega)}{V_3(\omega)} \tag{18}$$

This reference solution is in Fig. 10 compared with the voltage transfer function that can be calculated from the admittance matrix $\breve{\mathbf{Y}}^{(\text{short})}$ which has been derived from $\mathbf{Y}_{\text{meas}}^{(\text{long})}$ using the two alternative cable elimination methods. From the admittance definition (1) we obtain the voltage transfer function as

$$\breve{h}_{6,3}(\omega) = -\frac{\breve{y}^{(\text{short})}(6,3)}{\breve{y}^{(\text{short})}(3,3)} \tag{19}$$

Fig. 10 shows that the calculated voltage transfer function $\breve{h}_{6,3}(\omega)$ agrees much better with the direct measurement $h_{6,3}(\omega)$ (reference) when $\breve{\mathbf{Y}}^{(\text{short})}$ has been recovered from $\mathbf{Y}_{\text{meas}}^{(\text{long})}$ using the T-line method. In particular, the peak around 2 MHz is much more accurately represented, as well as the behavior at around 8 MHz.

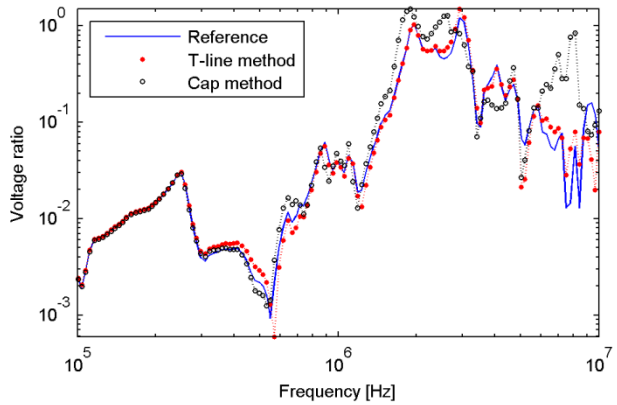

Fig. 10. Voltage transfer from terminal 3 to 6. Direct measurement (reference) and calculated response from the recovered $\breve{\mathbf{Y}}^{(\text{short})}$.

C. Simulated Time Domain Waveforms

The improvements in this example are even more striking in the time domain. The transfer functions $h_{6,3}(\omega)$ and $\breve{h}_{6,3}(\omega)$ were fitted in the band 5 Hz-10 MHz with a stable, high-order rational function using vector fitting [16-18]. (Passivity enforcement is not needed here since the transfer function does not interact with the system). In the time domain, a unit step voltage is applied to the transfer function input and the voltage response (output) is computed via recursive convolution [19].

Fig. 11 compares the step response of the model associated with the directly measured $h_{6,3}(\omega)$ with that of $\breve{h}_{6,3}(\omega)$ when cable compensation is not used. It is observed that the measurement cables lead to substantial errors in the simulated response, including an overestimate of the peak value and an underestimate of the frequency of the dominant 2 MHz component.

Fig. 12 shows the same result when $\breve{h}_{6,3}(\omega)$ has been obtained using the two cable compensation methods. It is observed that the T-line approach gives an excellent agreement with the reference solution whereas substantial errors remain with the Cap-method.

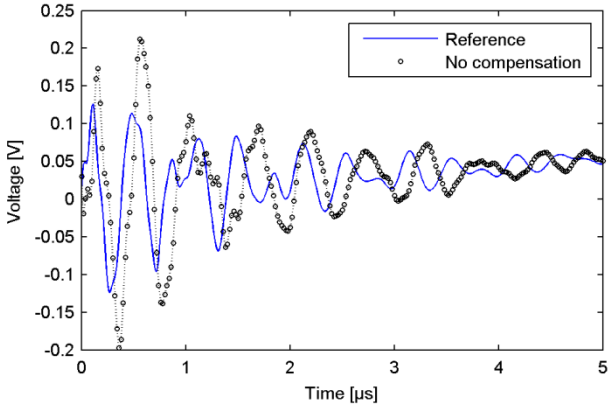

Fig. 11. Voltage response on terminal 6 when applying a unit step voltage to terminal 3. Simulated responses using rational models extracted from the

This article has been accepted for publication in a future issue of this journal, but has not been fully edited. Content may change prior to final publication. Citation information: DOI 10.1109/TPWRD.2016.2536704, IEEE Transactions on Power Delivery

measured $h_{6,3}(\omega)$ (reference) and from the calculated $\breve{h}_{6,3}(\omega)$. Without cable compensation.

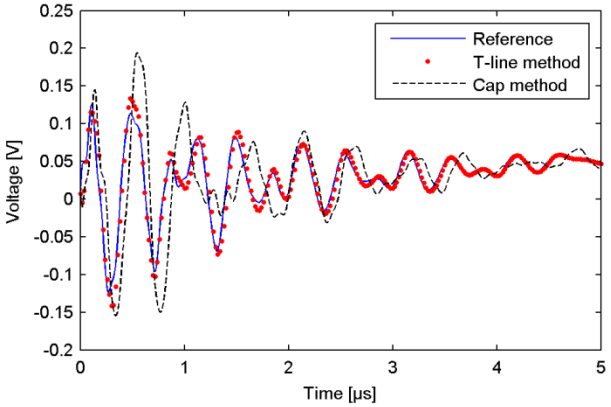

Fig. 12. Same result as in Fig. 11 when applying cable compensation.

D. Measured Time Domain Response

The very accurate result by the T-line method in Fig. 12 is in reality overly optimistic since the voltage transfer function was computed directly from the raw samples of $\breve{\mathbf{Y}}^{(\text{short})}$. In reality, the 6×6 $\breve{\mathbf{Y}}^{(\text{short})}$ is first fitted with a rational function approximation and thereafter subjected to passivity enforcement. In a time domain simulation, terminals 1, 2, 4, 5 will be grounded using small resistors and the modeling errors will show up in the simulation result, possibly with magnifications.

This scenario is investigated using the complete six-terminal model of the transformer obtained via vector fitting [16-18] and passivity enforcement using spectral residue perturbation [20]. A step-like voltage is applied to terminal 3 using a function generator and the voltage response on terminal 6 is measured. This result is compared against a simulation where the applied (measured) voltage is realized as an ideal voltage source.

Fig. 13 shows the measured voltage response (reference) and the simulated responses using the complete model with measurement cables eliminated by the two alternative approaches. As in the previous examples, the T-line method leads to a significantly more accurate result than the Cap-method. With the Cap-method, a high-frequency component is observed which has almost zero damping. For lower frequency components, there is no practical difference between the two approaches as shown in the extended time window in Fig. 14.

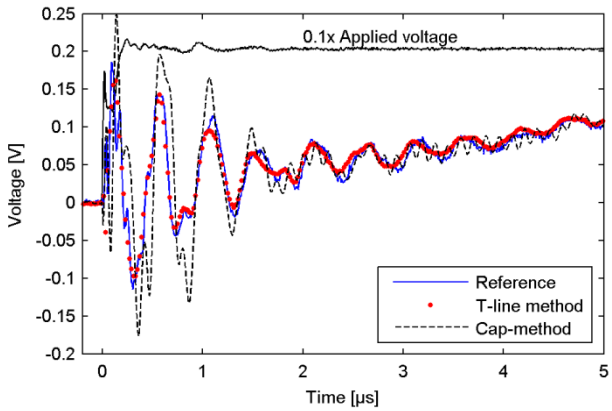

Fig. 13. Applying a near unit step voltage to terminal 3. Measured response (reference) and simulation using a rational model of $\breve{\mathbf{Y}}^{(\text{short})}$.

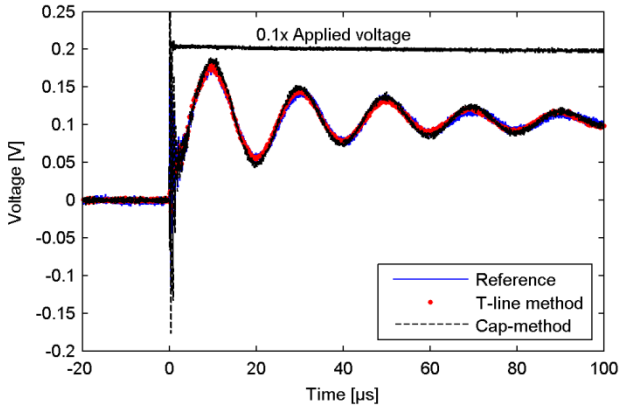

Fig. 14. Extended time window of Fig. 13.

E. Simulated Voltage Transfer in Opposite Direction

Similar investigations as in Section VII-C were made for the voltage transfer in the opposite direction. Fig. 15 shows the simulated voltage response on terminal 3 when applying a unit step voltage on terminal 6. The reference denotes the simulation result based on the the directly measured voltage transfer function with use of short cables. In this case, the voltage waveform is dominated by a slow oscillation of about 10 kHz. Still, the (long) measurement cables result in a significant reduction of the oscillation frequency due to the relatively small capacitance of the high-voltage winding. Both compensation methods lead to a similar result as the oscillation frequency is very small compared to the cable quarter wave frequency.

Fig. 16 shows the first 2.5 microseconds of the initial transient, revealing high-frequency oscillations above 1 MHz. The two compensation methods lead to a significant improvement in accuracy, in particular when using the T-line method.

This article has been accepted for publication in a future issue of this journal, but has not been fully edited. Content may change prior to final publication. Citation information: DOI 10.1109/TPWRD.2016.2536704, IEEE Transactions on Power Delivery

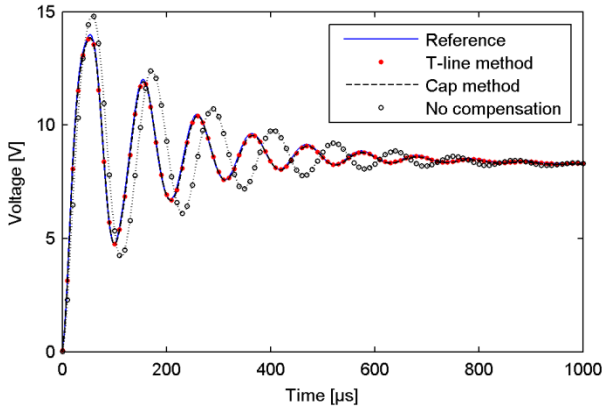

Fig. 15. Voltage response on terminal 3 when applying a unit step voltage to terminal 6. Simulated responses using rational models extracted from the measured $h_{3,6}(\omega)$ (reference) and from the calculated $\breve{h}_{3,6}(\omega)$.

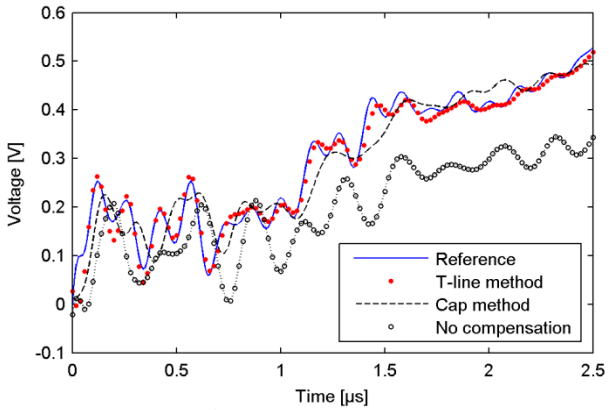

Fig. 16. Expanded view of Fig. 15.

VIII. Cable Modeling Using *S*-Parameters

The accuracy of the cable model used with the T-line method can potentially be improved by utilizing the *S*-parameter measurement capability of the VNA, in this case Agilent E5061B-3L5. To investigate this possibility, elements $S_{1,1}$ and $S_{2,1}$ were measured for the six cables in Table I. Fig. 17 shows the measured elements of the 6.2 m cable used for connecting terminal 1.

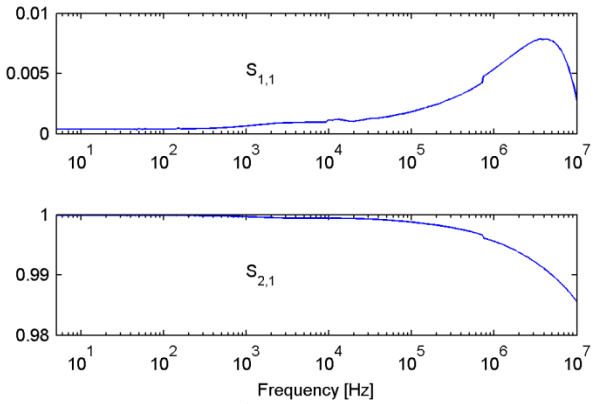

Fig. 17. Measured $S_{1,1}$ and $S_{2,1}$ of 6.2 m cable (magnitudes).

Using (14), the scattering matrix is converted into the associated admittance matrix, $\mathbf{Y}_{\text{cable}}$. The admittance matrix is subjected to eigenvalue decomposition into common mode and differential mode eigenvalues

$$\mathbf{T}^{-1}\mathbf{Y}_{\text{cable}}\mathbf{T} = \begin{bmatrix} \lambda_{\text{com}} & 0 \\ 0 & \lambda_{\text{diff}} \end{bmatrix} \tag{20}$$

using the transformation matrix

$$\mathbf{T} = \begin{bmatrix} 1 & 1 \\ 1 & -1 \end{bmatrix} \frac{1}{\sqrt{2}} \tag{21}$$

Fig. 18 shows the eigenvalues of $\mathbf{Y}_{\text{cable}}$. The same plot also shows the eigenvalues when $\mathbf{Y}_{\text{cable}}$ has been calculated from p.u.l. cable parameters using (5), along with a DC resistance for the centre conductor of 5.7 mΩ/m stated by the data sheet. It is observed that the eigenvalues are very close at frequencies above 10 kHz. At lower frequencies, the small (common mode) eigenvalue obtained from S-parameters becomes highly inaccurate in the relative sense as the expected capacitive behavior is lost. Since the transformer involves a delta winding, the capacitive behavior should be retained in order not to have a false ohmic connection to earth. This inaccuracy is rectified as follows. At 100 kHz, the common-mode eigenvalue has a linear behavior in the log-log plot and the real part is found to be much smaller than the imaginary part, indicating a capacitive behavior. Using a sample at this frequency, $\lambda_0(\omega_0)$, the samples for this eigenvalue at lower frequencies are replaced with

$$\lambda_{\text{com}}(\omega_k) \rightarrow j\frac{\omega_k}{\omega_0}\text{Im}\{\lambda_{\text{com}}(\omega_0)\} \tag{22}$$

where Im{} extracts the imaginary part. Fig. 19 shows the effect of rectifying the small eigenvalue.

Finally, the corrected $\mathbf{Y}_{\text{cable}}$ is recovered using the inverse transformation (23) with $\tilde{\lambda}_{\text{com}}$ denoting the corrected eigenvalue.

$$\mathbf{Y}_{\text{cable,corrected}} = \mathbf{T}\begin{bmatrix} \tilde{\lambda}_{\text{com}} & 0 \\ 0 & \lambda_{\text{diff}} \end{bmatrix}\mathbf{T}^{-1} \tag{23}$$

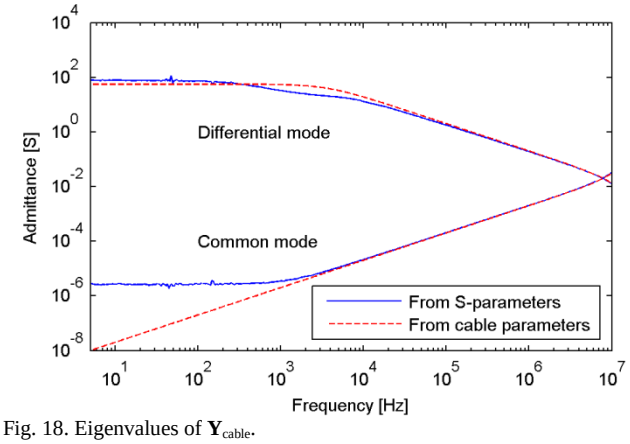

Fig. 18. Eigenvalues of $\mathbf{Y}_{\text{cable}}$.

This article has been accepted for publication in a future issue of this journal, but has not been fully edited. Content may change prior to final publication. Citation information: DOI 10.1109/TPWRD.2016.2536704, IEEE Transactions on Power Delivery

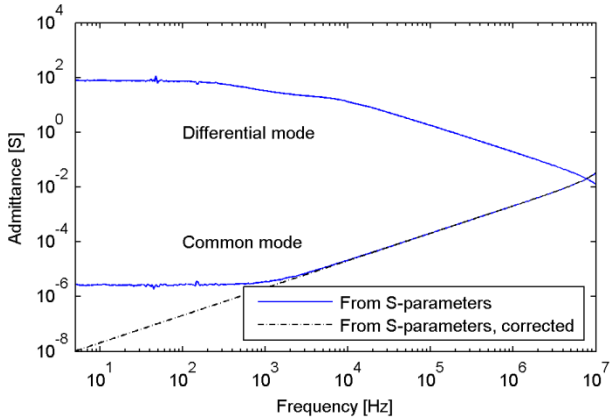

Fig. 19. Eigenvalues of $\mathbf{Y}_{\text{cable}}$ after correcting the common-mode eigenvalue.

Using the described procedure, an admittance representation $\mathbf{Y}_{\text{cable}}$ is established for each of the six measurement cables and used for removing the cable effect from the transformer measurements. Fig. 20 compares the frequency domain result for the voltage transfer from terminal 3 to 6, corresponding to Fig. 10 in Section VII. The results are seen to be nearly identical which is not surprising giving the close agreement at high frequencies in Fig. 18.

One technical detail is in order regarding Fig. 20. After removing the effect of the six cables, a 1-m cable model was inserted in series with terminals 3 and 6 to allow the comparison with the direct measurement (blue trace in Fig. 19). The model of the 1-m cable was obtained using p.u.l. parameters via (5).

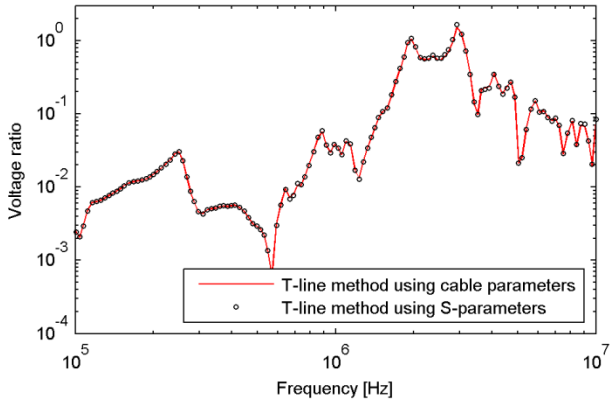

Fig. 20. Voltage transfer from terminal 3 to 6. Calculated from the recovered matrix $\tilde{\mathbf{Y}}_{\text{meas}}^{(\text{short})}$.

IX. Errors With the CAP-Method

A. Error Limits

The errors with the CAP-method depend on the cable length, the upper frequency limit considered, and on the loading impedance. In the case that the load is purely resistive and the cable resistance is negligible, the error can be plotted as function of the product between frequency and cable length. Fig. 21 shows the calculated relative error for alternative values of the load resistance, for a cable with assumed parameters Z_C=50 Ω, C=105 pF/m and R=0. For instance, with a 10 kΩ load resistance, the error is 30% at 1 MHz with a cable length of 5 meters.

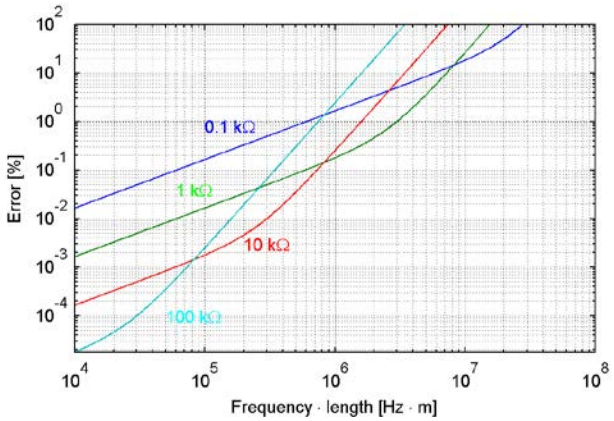

Fig. 21. Relative error in recovered resistive load by CAP-method.

B. Errors Induced by Passivity Enforcement

As mentioned in Section VI-B, cable elimination by the CAP-method often leads to passivity violations in the reduced admittance matrix. To demonstrate this effect, we emulate a measurement where the admittance of a 10 kΩ resistor has been measured using a 6-m cable having parameters R=0.0057 Ω/m, Z_C=50 Ω, C=105 pF/m. We next apply the CAP-method to eliminate the cable effect, and fit a rational model (2) to the reduced admittance using vector fitting [16]. This single-port model is finally subjected to passivity enforcement by the residue perturbation method described in [20].

Fig. 22 shows the result from this example. It is observed that the CAP-method substantially reduces the deviation of the reduced admittance (Y_{red}) from the actual load admittance, Y_{load}, giving a good agreement up to about 1 MHz. Y_{red} is seen to be fitted very accurately using vector fitting. However, the model has a negative term R_{-1} in (2). The subsequent passivity enforcement step is seen to introduce a quite large error in the recovered load admittance, even at low frequencies.

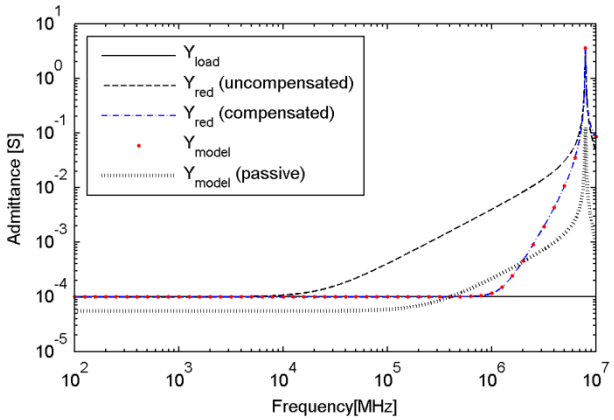

Fig. 22. Recovering the admittance of a 10 kΩ resistor using CAP method to compensate 6-m measurement cables. Effect of passivity enforcement on final model.

This article has been accepted for publication in a future issue of this journal, but has not been fully edited. Content may change prior to final publication. Citation information: DOI 10.1109/TPWRD.2016.2536704, IEEE Transactions on Power Delivery

X. Conclusion

Measurement cables can lead to substantial errors in the measurement of transformer admittance matrices at high frequencies. In this work a cable compensation method was introduced based on a transmission line representation of the measurement cables. The new method was found to greatly improve the accuracy of the corrected admittance matrix compared to an existing approach which considers only the cable shunt capacitances. The improvements were demonstrated for a measurement on a 45 MVA generator step-up transformer. Two alternative procedures were considered for establishing the transmission line model, using either per-unit-length parameters or S-parameter measurements. The procedures were found to give a similar accuracy for the extracted transformer model at high frequencies.

The admittance measurement method is quite general and can be used for the terminal characterization of other components as well, e.g. shunt reactors [21] and motors. Therefore, the presented cable elimination method can find use in many applications.

XI. Acknowledgment

The author appreciate the assistance of Oddgeir Rokseth during the measurements, as well as the Statkraft power station staff, in particular Olav Langseth.

XII. References

[1] I. Stevanovic, B. Wunsch, G.L. Madonna, S. Skibin, "High-frequency behavioral multiconductor cable modeling for EMI simulations in power electronics," *IEEE Trans. Industrial Informatics*, vol. 10, no. 2, pp. 1392-1400, May 2014.

[2] A. Morched, L. Marti, and J. Ottevangers, "A high frequency transformer model for the EMTP," *IEEE Trans. Power Delivery*, vol. 8, no. 3, pp. 1615-1626, July 1993.

[3] B. Gustavsen, "Wide band modeling of power transformers", *IEEE Trans. Power Delivery*, vol. 19, no. 1, pp. 414-422, Jan. 2004.

[4] A. Holdyk, B. Gustavsen, I. Arana, J. Holboell, "Wide band modeling of power transformers using commercial sFRA equipment", *IEEE Trans. Power Delivery*, vol. 29, no. 3, pp. 1446-1453, June 2014.

[5] M. Tiberg, D. Bormann, B. Gustavsen, C. Heitz, O. Hoenecke, G. Muset, J. Mahseredjian, and P.Werle, "Generic and automated simulation modeling based on measurements", in *Proc. International Conf. on Power Systems Transients* (IPST) 2007, 6p.D.

[6] Filipovic-Grcic, B. Filipovic-Grcic, I. Uglesic, "High-frequency model for the power transformer based on frequency-response measurements", *IEEE Trans. Power Delivery*, vol. 30, no. 1, pp. 34-42, Feb. 2015.

[7] B. Gustavsen and H.M.J. De Silva, "Inclusion of rational models in an electromagnetic transients program – Y-parameters, Z-parameters, S-parameters, transfer functions", *IEEE Trans. Power Delivery*, vol. 28, no. 2, pp. 1164-1174, April 2013.

[8] H.W. Dommel, ElectroMagnetic Transients Program. Reference Manual (EMTP Theory Book), Bonneville Power Administration, Portland, 1986.

[9] CIGRE JWG A2/C4.39, "Electrical transient interaction between transformers and the power system", Technical Report 577A/B, April 2014.

[10] IEEE Std C57.142-2010, IEEE Guide to describe the occurrence and mitigation of switching transients induced by transformers, switching device, and system interaction.

[11] B. Gustavsen, "Study of transformer resonant overvoltages caused by cable-transformer high frequency interaction", *IEEE Trans. Power Delivery*, vol. 25, no. 2, pp. 770-779, April 2010.

[12] A. Borghetti, A. Morched, F. Napolitano, C.A. Nucci, "Lightning-induced overvoltages transferred through distribution power transformers", *IEEE Trans. Power Delivery*, vol. 24, no. 1, pp. 360-372, Jan. 2009.

[13] G. Kron, *Tensor analysis of networks*, John Wiley and Sons, 1965.

[14] K. Kurokawa, "Power waves and the scattering matrix", *IEEE Trans. Microwave Theory and Techniques*, vol. 13, no. 2, pp. 194-202, 1965.

[15] A. Ametani, "A general formulation of impedance and admittance of cables," *IEEE Trans. Power Apparatus and Systems*, no. 3, pp. 902–910, 1980.

[16] B. Gustavsen and A. Semlyen, "Rational approximation of frequency domain responses by vector fitting", *IEEE Trans. Power Delivery*, vol. 14, no. 3, pp. 1052-1061, July 1999.

[17] B. Gustavsen, "Improving the pole relocating properties of vector fitting", *IEEE Trans. Power Delivery*, vol. 21, no. 3, pp. 1587-1592, July 2006.

[18] D. Deschrijver, M. Mrozowski, T. Dhaene, and D. De Zutter, "Macromodeling of multiport systems using a fast implementation of the vector fitting method", *IEEE Microwave and Wireless Components Letters*, vol. 18, no. 6, pp. 383-385, June 2008.

[19] A. Semlyen and A. Dabuleanu, "Fast and accurate switching transient calculations on transmission lines with ground return using recursive convolutions", *IEEE Trans. Power Apparatus and Systems*, vol. 94, pp. 561-575, March/April 1975.

[20] B. Gustavsen, "Fast passivity enforcement for pole-residue models by perturbation of residue matrix eigenvalues", *IEEE Trans. Power Delivery*, vol. 23, no. 4, pp. 2278-2285, October 2008.

[21] B. Gustavsen, M. Runde, T. Ohnstad, "Wideband modeling, field measurement, and simulation of a 420-kV variable shunt reactor", *IEEE Trans. Power Delivery*, vol. 30, no. 3, pp. 1594-1601, June 2015.

XIII. Biographies

Bjørn Gustavsen (M'94–SM'2003–F'2014) was born in Norway in 1965. He received the M.Sc. degree and the Dr.Ing. degree in Electrical Engineering from the Norwegian Institute of Technology (NTH) in Trondheim, Norway, in 1989 and 1993, respectively. Since 1994 he has been working at SINTEF Energy Research where he is currently Chief Scientist. His interests include simulation of electromagnetic transients and modeling of frequency dependent effects. He spent 1996 as a Visiting Researcher at the University of Toronto, Canada, and the summer of 1998 at the Manitoba HVDC Research Centre, Winnipeg, Canada. He was a Marie Curie Fellow at the University of Stuttgart, Germany, August 2001–August 2002. He is convenor of CIGRE JWG A2/C4.52.